

RESEARCH ARTICLE | NOVEMBER 01 2024

Microscopic mechanism of water-assisted diffusional phase transitions in inorganic metal halide perovskites

Special Collection: [2024 JCP Emerging Investigators Special Collection](#)

Jialin Liu ; Xiangming Hao; Marijn A. van Huis ; Zhaochuan Fan  

 Check for updates

J. Chem. Phys. 161, 174705 (2024)

<https://doi.org/10.1063/5.0220702>



Articles You May Be Interested In

Phase stability investigation of CsPbI₃ perovskite for solar cell application

AIP Conference Proceedings (March 2021)

Interface engineering of CsPbI₃-black phosphorus van der Waals heterostructure

Appl. Phys. Lett. (January 2018)

Molecular dynamics simulation for phase transition of CsPbI₃ perovskite with the Buckingham potential

J. Chem. Phys. (September 2024)



The Journal of Chemical Physics

Special Topics Open for Submissions

[Learn More](#)

Microscopic mechanism of water-assisted diffusional phase transitions in inorganic metal halide perovskites

Cite as: J. Chem. Phys. 161, 174705 (2024); doi: 10.1063/5.0220702

Submitted: 5 June 2024 • Accepted: 12 September 2024 •

Published Online: 1 November 2024



View Online



Export Citation



CrossMark

Jialin Liu,¹  Xiangming Hao,¹ Marijn A. van Huis,²  and Zhaochuan Fan^{1,a)} 

AFFILIATIONS

¹Suzhou Institute of Nano-Tech and Nano-Bionics, Chinese Academy of Sciences, Suzhou 215123, People's Republic of China

²Soft Condensed Matter, Debye Institute for Nanomaterials Science, Utrecht University, 3584CC Utrecht, The Netherlands

Note: This paper is part of the 2024 JCP Emerging Investigators Special Collection.

a) Author to whom correspondence should be addressed: zcfan2021@sinano.ac.cn

ABSTRACT

The stability of perovskite materials is profoundly influenced by the presence of moisture in the surrounding environment. While it is well-established that water triggers and accelerates the black–yellow phase transition, leading to the degradation of the photovoltaic properties of perovskites, the underlying microscopic mechanism remains elusive. In this study, we employ classical molecular dynamics simulations to examine the role of water molecules in the yellow–black phase transition in a typical inorganic metal halide perovskite, CsPbI₃. We have demonstrated, through interfacial energy calculations and classical nucleation theory, that the phase transition necessitates a crystal–amorphous–crystal two-step pathway rather than the conventional crystal–crystal mechanism. Simulations for CsPbI₃ nanowires show that water molecules in the air can enter the amorphous interface between the black and yellow regions. The phase transition rate markedly increases with the influx of interfacial water molecules, which enhance ion diffusivity by reducing the diffusion barrier, thereby expediting the yellow–black phase transition in CsPbI₃. We propose a general mechanism through which solvent molecules can greatly facilitate phase transitions that otherwise have prohibitively high transition energies.

Published under an exclusive license by AIP Publishing. <https://doi.org/10.1063/5.0220702>

I. INTRODUCTION

Perovskite materials are highly regarded for their optoelectronic properties, yet their low thermodynamic stability has posed a significant challenge in their advancement and implementation.^{1–3} Inorganic metal halide perovskites (MHPs), such as CsPbI₃ and CsSnI₃, exhibit optical activity in the high-temperature perovskite black α phase, but under ambient conditions, their thermodynamically stable state is the optically inactive non-perovskite yellow δ phase.^{4–7} The structural disparity between the black and yellow phases of inorganic MHPs is considerable, and the black–yellow ($B \leftrightarrow Y$) phase transition involves overcoming substantial energy barriers (1–2 eV), rendering the transition path complex.^{8–11} Density functional theory (DFT) calculation studies have predicted that CsPbI₃ transitioning from the black phase to the yellow phase via a direct one-step pathway requires overcoming a barrier of 68 meV/atom,¹² which can be reduced to 31 meV/atom through

a multi-step process involving four transition states and three metastable states.¹³ Classical molecular dynamics (MD) simulations have predicted a different transition mechanism that the yellow phase of CsPbI₃ transforms into a liquid-like disordered structure at high temperatures before recrystallizing into the black phase.¹⁴ Experimental validation of the atomic-level transition mechanism is currently infeasible, leaving the underlying mechanism unclear.

Water plays a crucial role in the $B \leftrightarrow Y$ phase transition in MHPs.^{15–21} Under dry conditions, rapid cooling can maintain the material in the metastable black β and γ phases without transitioning to the yellow phase.^{4,16,22} Experimental evidence suggests that without water molecules, defect introduction via laser irradiation is insufficient to induce the $B \rightarrow Y$ phase transition.¹⁶ However, under humid conditions, water molecules in the air trigger the nucleation process of the $B \leftrightarrow Y$ transition, and the transition is highly sensitive to environmental humidity.^{17–19} As humidity increases from 53% to 73%, the nucleation barrier of yellow-CsPbI₃ decreases from

1.34 to 0.57 eV.⁹ Additionally, the rate of the B → Y phase transition in CsPbI₃ nanowires exhibits an instantaneous response to environmental humidity, enabling real-time control of the transition rate by regulating environmental humidity.²⁰ A differential scanning calorimetry experiment has confirmed that the enthalpy change of the B → Y phase transition in CsPbI₃ is independent of water content, suggesting that water molecules catalyze the phase transition process rather than forming H₂O adducts.²¹

Molecular simulations have been widely used to study the role of water molecules in the B ↔ Y phase transition of MHPs.^{23–35} DFT calculations show that the addition of a water molecule to a 20-atom CsPbI₃ system reduces the energy barrier of the B ↔ Y phase transition by 10 meV/atom through the one-step pathway.³³ However, the direct penetration of water molecules from the crystal surface into the crystal interior requires overcoming a larger energy barrier of 0.46 eV, making it less likely.³⁰ On the other hand, the energy barrier for water molecules to enter the perovskite material from grain boundaries is much smaller.³⁰ MD simulations of the water/MAPbI₃ and water/CsPbI₃ two-phase systems suggest that surface I ions can dissolve into the water layer, resulting in the creation of iodine vacancies.^{28,29} Consequently, it has been suggested that these vacancies could decrease the energy barrier for the B ↔ Y phase transition.^{9,29,35} Yet, prior computational studies have been constrained by the spatial and temporal scale of the examined systems, indirectly inferring the mechanism of the water-assisted B ↔ Y phase transition from simulation outcomes of small-scale systems. Consequently, simulations for large systems with long dynamics are necessary to replicate these phase transitions and elucidate the microscopic mechanism of the water-assisted B ↔ Y phase transition.

This study employs empirical force fields and MD simulations to elucidate how water molecules assist the B ↔ Y phase transitions in inorganic MHPs at the atomistic level. By employing an efficient rigid ion model capable of accurately capturing the physics of the MHP–water system, we are able to model the microsecond-scale dynamics of 16 nm-long CsPbI₃ nanowires in a humid environment. We select the typical inorganic MHP CsPbI₃ as the model system, but the conclusions drawn are equally applicable to similar perovskite systems. Through analysis of the nucleation barriers, we conclude that the B ↔ Y phase transition in perovskite materials involves a two-step crystal–amorphous–crystal (C–A–C) mechanism. Furthermore, through analysis of the phase transition barriers, interface ion diffusion barriers, and simulation trajectories in systems with different water contents, we find that water molecules enhance the diffusion rate of interface ions by binding with interface cations and releasing anions, thereby lowering the phase transition barrier and accelerating the transition process.

II. RESULTS

A. Two-step C–A–C transition mechanism

We first discuss the mechanism of the B ↔ Y phase transition occurring in MHPs. Previous studies based on DFT calculations have proposed both one-step and multi-step transition pathways for the B → Y phase transition in CsPbI₃.^{12,13,36} However, the solid–solid phase transition mechanism cannot rely solely on calculating the minimum energy barrier per atom for homogenous transitions;

the nucleation process during the transition must also be considered. Additionally, these studies were based on the assumption that the transition states and metastable phases along the pathway are crystals [i.e., the crystal–crystal (C–C) transition mechanism]. We argue that the B ↔ Y phase transition in CsPbI₃ or other inorganic perovskite materials follows a two-step C–A–C mechanism.^{14,37,38} During the B ↔ Y phase transition, the nucleation and propagation stages can be effectively distinguished,⁹ and both can be understood using classical nucleation theory (CNT).³⁹ If the transition occurs via the direct C–C transition pathway, the nucleation barrier would be significantly higher than the corresponding values for a feasible phase transition. Assuming the formation of a spherical nucleus with a diameter of R in the transitioning crystal, according to CNT, the energy cost ΔG for generating this nucleus is given by³⁹

$$\Delta G = \frac{4}{3}\pi R^3 \left(\frac{\Delta\mu}{v} + \frac{3\sigma}{R} \right), \quad (1)$$

where v represents the molar volume of the nucleus, $\Delta\mu$ represents the molar free energy difference between the black and yellow phases, and σ represents the interfacial energy of the interface between the nucleus and transitioning crystal. We use the energy difference of 26 meV/atom between the black and yellow phases of CsPbI₃ at 0 K, determined by DFT-RPA calculations, as $\Delta\mu$.⁴⁰ This energy difference represents the maximum driving force for the B → Y phase transition in CsPbI₃, as an increase in temperature decreases the free energy difference between the black and yellow phases. Concerning the driving force behind the reverse Y → B phase transition, free energy calculations using both classical force field³⁸ and MLFF⁴¹ confirm that the free energy difference between the two phases—where the Gibbs free energy of the black phase is lower than that of the yellow phase—can approach the magnitude of the energy difference between the phases at 0 K as the temperature increases. Consequently, the nucleation barrier curve for the $\delta \rightarrow \alpha$ phase transition is expected to resemble that of the $\gamma \rightarrow \delta$ phase transition.

The free energy difference between the bulk black and yellow phases provides the driving force for nucleation, while the interfacial energy impedes the formation of nuclei. We verify that the classical force field can accurately describe the interfacial energy between different structures (supplementary material, Table I). For the one-step C–C transition mechanism, σ corresponds to the interfacial energy of the black/yellow (B/Y) interface [Fig. 1(a), red box], calculated to be 1.4 eV/nm² (supplementary material, computational methods, force field validation, Table I, and Fig. S1). The red solid line in Fig. 1(b) shows the variation of ΔG with R , predicting that if the B ↔ Y phase transition occurs via the one-step C–C transition, the critical radius of the nucleus is 5 nm, and the nucleation barrier reaches 150 eV! For the multi-step C–C phase transition mechanism,¹³ σ can be reduced to 0.8 eV/nm² [Fig. 1(a), yellow box],⁴² but the corresponding nucleation barrier still reaches 25 eV [yellow line in Fig. 1(b)]. Such high nucleation barriers are far above the maximum barrier allowed by thermally activated nucleation processes ($\sim 80 k_B T$),⁴³ making the possibility of phase transition via the C–C mechanism extremely low.

On the other hand, an amorphous structure in a transition/metastable state can effectively reduce the interfacial energy, thereby lowering the nucleation barrier. The calculated interfacial

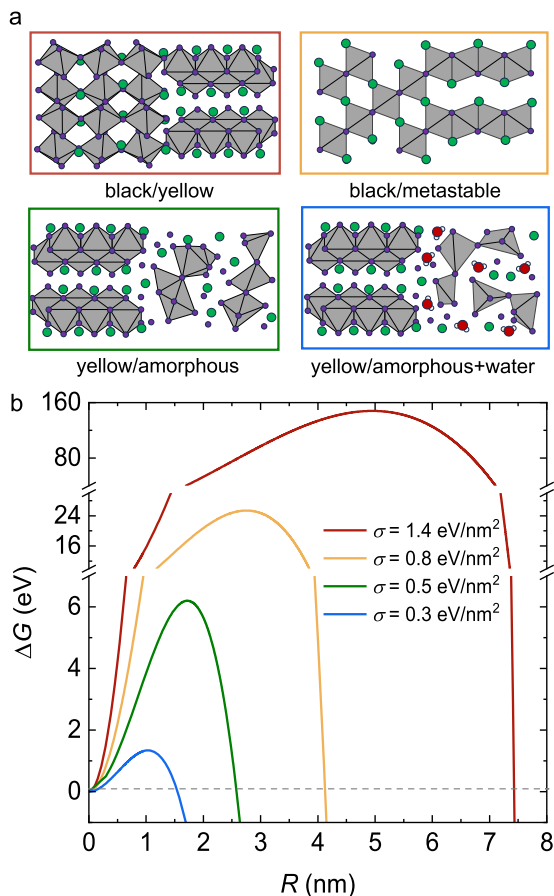


FIG. 1. B \leftrightarrow Y transitions in CsPbI₃ follow the two-step C–A–C mechanism. (a) Different crystal/crystal (B/Y and B/MS) and crystal/amorphous (Y/A and Y/A + w) interfaces for interfacial energy calculations. Green, gray, purple, red, and white spheres are Cs, Pb, I, O, and H, respectively. (b) The energy cost for nucleation ΔG with different σ as a function of nucleus radius R calculated according to the classical nucleation theory. The σ values of 1.4, 0.8, 0.5, and 0.3 eV/nm² correspond to the interfacial energies of the B/Y, B/MS, Y/A, and Y/A + w interfaces, respectively.

energy of the yellow/amorphous (Y/A) interface [Fig. 1(a), green box] is ~ 0.5 eV/nm² (supplementary material, computational methods, force field validation, Table I and Fig. S1), corresponding to a nucleation barrier of about 6 eV [green line in Fig. 1(b)]. This value is close to the maximum barrier allowed for nucleation at the B \leftrightarrow Y phase transition point (4 eV ≈ 80 $k_B T$, $T = 580$ K). By introducing water molecules into the amorphous region [Fig. 1(a), blue box], σ is further reduced to 0.3 eV/nm² (supplementary material, computational methods, force field validation, Table I and Fig. S1), corresponding to a nucleation barrier of 1.4 eV [blue line in Fig. 1(b)]. This nucleation barrier is lower than the maximum barrier allowed for the nucleation processes at room temperature (2 eV ≈ 80 $k_B T$, $T = 300$ K). Our calculations demonstrate that the B \leftrightarrow Y phase transition in CsPbI₃ cannot occur via C–C but can occur via the two-step C–A–C pathway.

In CNT, only the influence of transition/metastable states on interfacial energy is considered, neglecting the energy barrier generated by the transition states themselves. Estimated critical nucleus radii for the B \leftrightarrow Y phase transition via one-step and multi-step C–C pathways are 5.1 and 2.8 nm, housing ~ 11 000 and 1800 ions within the nucleus. DFT calculations yield energy barriers of 68 and 31 meV per atom for one-step¹² and multi-step¹³ transitions, resulting in total barriers of about 800 and 60 eV, respectively. These high transition barriers reaffirm the infeasibility of the B \leftrightarrow Y phase transition via the C–C pathway. Critical radii for amorphous nuclei with and without water are 1.1 and 1.7 nm, respectively, hosting 100 and ~ 400 ions. The energy difference between the amorphous and yellow phase CsPbI₃ is estimated at about 55 meV per atom using MD simulations, resulting in a transition barrier of 23 eV for crossing with anhydrous amorphous CsPbI₃ as the transition state. This high energy barrier also prevents the occurrence of the B \rightarrow Y transition via the C–A–C pathway, consistent with experimental observations that CsPbI₃ undergoes the $\alpha \rightarrow \beta \rightarrow \gamma$ upon cooling under dry conditions.^{4,16} However, this does not rule out the possibility that the Y \rightarrow B phase transition occurs via the C–A–C pathway under high-temperature conditions. Increasing the temperature enhances the driving force of the Y \rightarrow B transition, leading to reduced critical nucleus size and lower nucleation and transition barriers (as in $k_B T$). Direct calculation of the energy difference for hydrated amorphous CsPbI₃ with respect to the yellow phase is infeasible. However, it is evident that water can prompt the dissolution and degradation of CsPbI₃,¹⁵ rendering the transition from the yellow phase to the amorphous structure likely to be spontaneous.

B. Water molecules assisting the phase transition by entering the B/Y interface

Experimental observations of the B \leftrightarrow Y phase transitions in CsPbI₃ typically employ nanowires as material models.^{20,44,45} We constructed three different CsPbI₃ nanowire models to understand the water–MHP interactions: the black phase [Fig. 2(a)], the yellow phase [Fig. 2(b)], and a half-black and half-yellow (B–Y) structure [Fig. 2(c)]. For the B–Y nanowire, the (100) face of the black phase contacts the (100) face of the yellow phase, as this B/Y interface has been confirmed experimentally.⁴⁶ 1500 water molecules were randomly placed near the nanowire surface in these three systems. MD simulations were performed at 300 K [Figs. 2(a)–2(c) left panels] and 600 K [Figs. 2(a)–2(c) right panels] and 1 atm for 1 μ s. The simulation results show that water molecules do not penetrate the nanowires with pure yellow or black phases [Figs. 2(a) and 2(b)]. They form a thin water layer on the surfaces at low temperatures or mostly water vapor at high temperatures, with only a few water molecules adsorbed on the nanowire surface. This observation agrees with *in situ* ambient pressure x-ray photoemission spectroscopy experiments on CsPbI₃.²⁹ Since air molecules were not considered in our nanowire system, the water content cannot be directly correlated with the relative humidity in experimental conditions. However, the water content used in our simulations is appropriate. An insufficient amount of water molecules cannot effectively accelerate the phase transition, whereas an excessive amount can lead to the dissolution of CsI, prompting the transformation from CsPbI₃ to CsPb₂I₅ and eventually to PbI₂.²⁴ The water content in our simulated system is sufficient to effectively accelerate

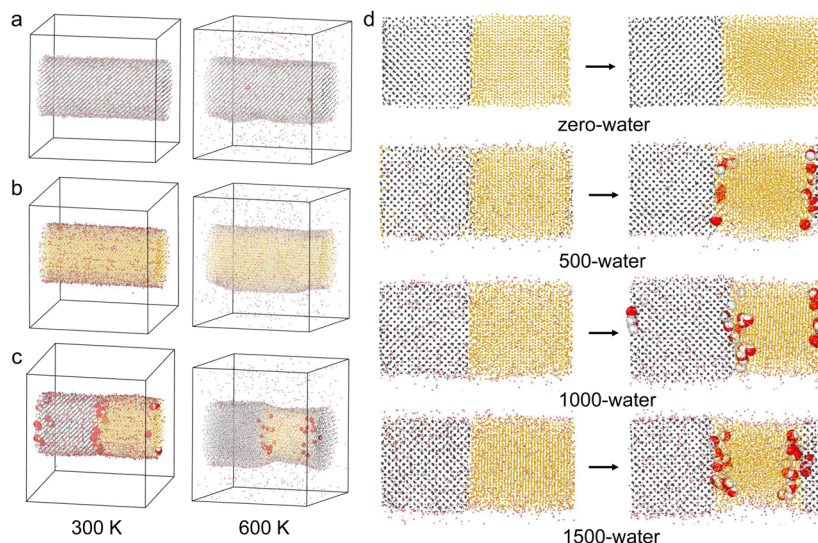


FIG. 2. Water-assisted B \rightarrow Y phase transition in CsPbI₃ nanowires. (a)–(c) MD simulations for CsPbI₃ nanowires in (a) pure black and (b) yellow phases, and with (c) a half-black half-yellow (B–Y) structure with 1500 water molecules at 300 and 600 K. (d) Initial and final configurations of 1 μ s MD simulations for a B–Y nanowire with zero, 500, 1000, and 1500 water molecules at 600 K. Only cations (Cs and Pb) in CsPbI₃ are shown for clarity. Yellow and gray indicate the yellow and black phases, respectively. The water molecules penetrating the nanowires are displayed with a larger size.

the B \rightarrow Y phase transition of CsPbI₃ without significantly degrading or damaging the nanowires. However, for the B–Y nanowire, some water molecules can penetrate the nanowire at the B/Y interface [Fig. 2(c)], implying that during the B \leftrightarrow Y phase transitions, once the nuclei with the competing structure form, water molecules do not merely adsorb on the nanowire surface; they can interact with CsPbI₃ by entering the B/Y interfaces. Water molecules are capable of migrating at the interfaces and into the vacuum (supplementary material, Fig. S4).

We now focus on the propagation process in the Y \leftrightarrow B phase transitions. Research has utilized metadynamics simulations to reproduce the B–Y phase transition processes in CsPbI₃ and FAPbI₃.^{47,48} However, these studies are based on small-scale systems and specific collective variables (CVs). Consequently, the phase transition mechanisms elucidated may not account for the possibility of nucleation and could be biased by the choice of CVs. Unbiased microsecond-scale MD simulations can only reproduce the Y \rightarrow B phase transition at high temperatures^{14,37,38} and not the slower B \rightarrow Y phase transition at low temperatures (supplementary material, Fig. S2). However, the growth of the yellow phase from hydrated amorphous CsPbI₃ is confirmed by MD simulations (supplementary material, Fig. S2). Since both B \leftrightarrow Y phase transitions should follow the two-step C–A–C mechanism and water affects the transitions at the amorphous B/Y interface, the water-assisted mechanism in the Y \rightarrow B phase transition process should be consistent with the low-temperature reverse B \rightarrow Y transition. We constructed the B–Y nanowire systems with different numbers of water molecules (0, 500, 1000, and 1500) and performed MD simulations at 600 K for 1 μ s [Fig. 2(d)]. Our simulations show that the number of penetrating water molecules increases with the total number of water molecules (supplementary material, Fig. S3). Figure 2(d) shows that Y \rightarrow B phase transitions are taking place in

the simulations, with a significant contraction of the yellow phase region and a notable expansion of the black phase region. Here, we define the transition rate ν as

$$\nu = \frac{L}{2} \frac{d(n_B/n_{\text{tot}})}{dt}, \quad (2)$$

where n_B represents the number of cations in the black phase, n_{tot} is the total number of cations, L is the x -dimension of the simulation box, and t is the time. The rate of the Y \rightarrow B phase transition increases significantly with the number of water molecules (supplementary material, Fig. S3). The 1500-water system shows the fastest Y \rightarrow B phase transition with a transition rate $\nu = 0.144$ m/s, approximately three times faster than the zero-water system (supplementary material, Fig. S3). Note that water molecules mainly accumulated in the B/Y interface area during the phase transition at 600 K [Fig. 2(d)], indicating that interfacial water plays a key role in accelerating the phase transition.

C. Kinetics of the water-assisted phase transition

In experiments, CsPbI₃ nanowires typically have diameters greater than 100 nm and exhibit properties more akin to bulk materials. Therefore, we also constructed a B–Y bulk material model with three-dimensional periodic boundary conditions^{49,50} (supplementary material, computational methods and Fig. S4). The main advantages of using the bulk material model in simulations are the elimination of the surface effects on phase transitions and the convenience of sampling. In the bulk models, 0, 50, 100, and 150 water molecules were placed at the B/Y interfaces for each system (0, 25, 50, and 75 water molecules per interface), and MD simulations were performed for each system at 700 K for 1.5 μ s. Similar to the nanowire simulations, the Y \rightarrow B transition rate in the B–Y

bulk systems also shows sensitive dependence on the water content. For example, while the zero-water system shows minimal change, the 150-water system shows nearly a complete $Y \rightarrow B$ phase transition in 320 ns (supplementary material, Fig. S4). During the phase transition, we observed that water molecules primarily accumulate at the interface, where they can move along the interface and undergo overall translation as the interface propagates. However, these water molecules rarely penetrate the crystalline region (supplementary material, Fig. S6). Figure 3(a) shows the time evolution of the fraction of the black phase with different water contents at 700 K. Here, the water content is given in water areal density, $\rho = n_W/2S$, where n_W is the number of water molecules and S is the area of the y - z plane of the simulation box. Figure 3(b) shows v as a function of ρ at different temperatures. For a particular simulated temperature, the transition rate increased nonlinearly with the number of water molecules [Figs. 3(a) and 3(b) and supplementary material, Fig. S5]. For instance, the transition rate in the zero-water system is 0.48×10^{-3} m/s at 700 K, while that in the 150-water system is 5.6×10^{-3} m/s at 700 K, an order of magnitude higher. We have also constructed distinct B/Y interfaces [the γ -(010) surface contacts with the δ -(010) surface], and MD simulations yielded similar results as those observed at the B/Y interface (supplementary material, Fig. S5).

Assuming that the energy barrier of the $Y \rightarrow B$ phase transition (ΔE_{tran}) does not significantly change with temperature, we can calculate ΔE_{tran} using the transition rates at various temperatures

near 710 K (700, 710, and 720 K; see supplementary material, Fig. S5) with the Arrhenius equation

$$v = A \exp(-\Delta E_{\text{tran}}/k_B T), \quad (3)$$

where A is the pre-exponential factor. Figure 3(c) shows the linear fit between $\ln(v)$ and $1/T$ for systems with different water contents (ρ). Water molecules act as catalysts, and increasing their concentration enhances the interfacial ion diffusion coefficient, promotes effective collisions, and subsequently elevates the pre-exponential factor A in the Arrhenius equation.⁵¹ Figure 3(d) shows ΔE_{tran} as a function of ρ at 710 K. The results indicate that ΔE_{tran} decreases as ρ increases. Compared to the zero-water system in which ΔE_{tran} is 1.63 eV, ΔE_{tran} decreases to 1.34 eV when ρ reaches 2.17 nm^{-2} . In general, our calculated energy barriers of transitions in CsPbI_3 are consistent with experimental observations that the water molecules accelerate the $B \leftrightarrow Y$ transitions in perovskite materials by decreasing the transition barriers. However, it is challenging to accurately measure the relationship between the transition barrier and the water content in high-temperature experiments.^{8,14} Unlike our simulations, experiments control the environmental humidity rather than the exact number of water molecules at the CsPbI_3 B/Y interface, which varies significantly with temperature.^{9,20}

The mechanism of the water-assisted $Y \rightarrow B$ phase transition in CsPbI_3 strongly relates to the diffusional nature of this transition.

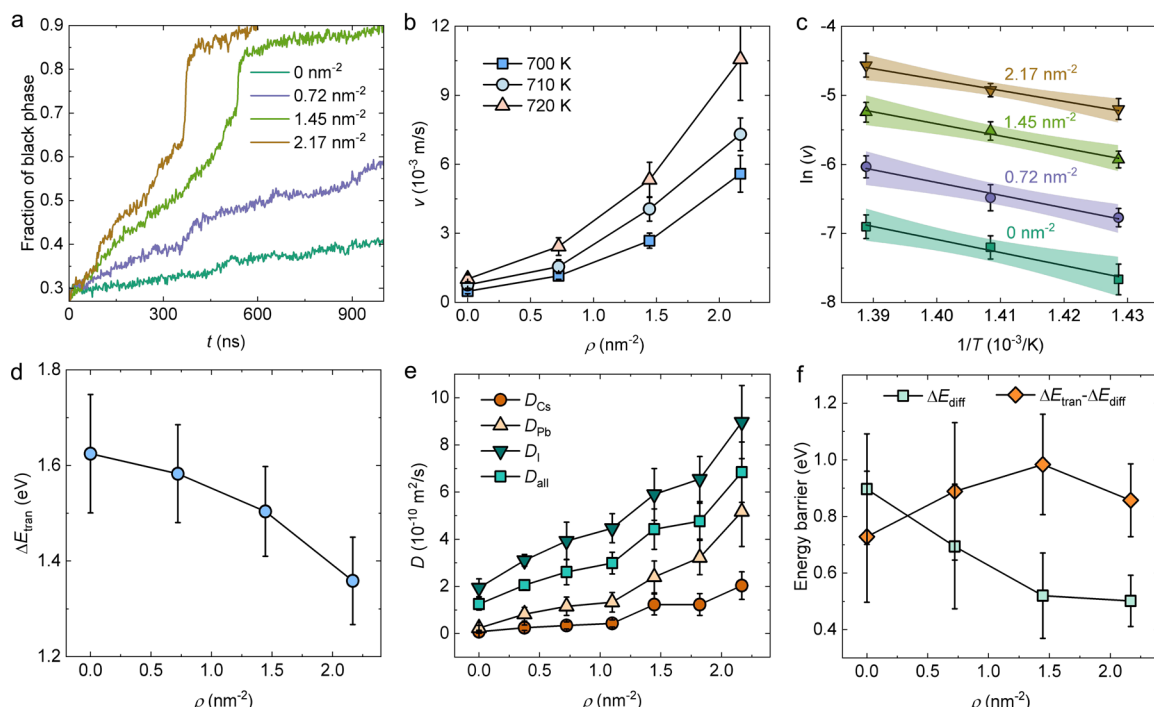


FIG. 3. Effects of the interfacial water on the $Y \rightarrow B$ transition. (a) Time evolution of the fraction of black phase with different numbers of water molecules (shown in areal density ρ) during the $Y \rightarrow B$ phase transitions at 700 K. (b) $Y \rightarrow B$ transition rates as a function of ρ at different temperatures. (c) Arrhenius plot of MD simulation data for systems with different interfacial water densities. The shaded regions show the 85% confidence interval of the fits. (d) Transition barrier ΔE_{tran} as a function of ρ . (e) Diffusion coefficients of the interfacial ions D as a function of ρ . (f) Diffusion barrier of interfacial ions ΔE_{diff} and the difference between transition and diffusion barrier ($\Delta E_{\text{tran}} - \Delta E_{\text{diff}}$) as a function of ρ .

In these typical non-martensitic phase transitions, the ability of ions to diffuse at the interface directly determines the rate of phase propagation. Figure 3(e) shows the diffusion coefficients (D) of ions at the B/Y interface at 710 K as a function of ρ (supplementary material, computational methods and Fig. S6). The diffusion coefficient for each ion and the total diffusion coefficient both increase with ρ . In the absence of water, the diffusion coefficient for the anions ($D_I = 1.94 \times 10^{-10}$ m²/s) is larger than those for the cations ($D_{Cs} = 0.08 \times 10^{-10}$ m²/s; $D_{Pb} = 0.24 \times 10^{-10}$ m²/s). This result agrees with DFT calculations reporting that I ions diffuse more readily than cations.^{52,53} To calculate the energy barriers of ion diffusion ΔE_{diff} , we again applied the Arrhenius equation

$$D = A' \exp(-\Delta E_{diff}/k_B T), \quad (4)$$

where A' is the diffusion rate extrapolated to infinite temperature. The linear fit between $\ln(D)$ and $1/T$ for systems with different amounts of water is shown in supplementary material, Fig. S7. Figure 3(f) shows the diffusion barrier ΔE_{diff} and the difference between the transition and diffusion barriers $\Delta E_{tran} - \Delta E_{diff}$ as a function of ρ . ΔE_{diff} shows similar trends as ΔE_{tran} , which decreases as ρ increases. This difference in energy barriers may be closely related to the solidification mechanism of non-metallic systems. Unlike metallic systems, non-metallic systems tend to form flat solid/liquid interfaces during solidification, effectively reducing the number of dangling bonds.⁴³ Consequently, the solidification growth mode of non-metallic systems is primarily characterized by step growth or spiral growth, accompanied by the formation of disc-shaped nuclei at the interface.⁴³ We speculate that the energy barrier associated with this nucleation process primarily contributes to $\Delta E_{tran} - \Delta E_{diff}$, and this process is not influenced by the water content. Therefore, our simulations prove that the reduction of the transition barrier by water molecules corresponds to the lowering of the ion diffusion barrier at the B/Y interface.

D. Water-ion structure at the B/Y interface

A closer inspection of the ion and water motion at the B/Y interfaces reveals that the water molecules are able to bind with Cs and Pb ions, thus releasing I ions that are originally bound to the cations [Fig. 4(a) and supplementary material, Movie S1]. In the pure black and yellow phases, Cs is coordinated with 12 and 9 I, respectively, and Pb is coordinated with 6 I. We sampled the coordination numbers of ions at the B/Y interface (supplementary material, computational methods). In the zero-water system, the average coordination number of Pb (i.e., the number of I surrounding Pb) at the interface is 6.1, and that of Cs is 10.2. As shown in Fig. 4(b), the coordination numbers of both Cs and Pb slightly decrease as the water content increases. We calculated the probabilities of different binding situations ($I_{n-x}W_x$, where n is the total number of I and water molecules bound to a cation, x is the number of water molecules bound to the cation) for cations at the interface. Figures 4(c) and 4(d) compare the probability distribution of cation binding situations in the zero- and 150-water systems. Both systems show similar probability distributions of the total coordination numbers (n) of Pb [Fig. 4(c)] and Cs [Fig. 4(d)]. However, the numbers of I ions surrounding cations in the 150-water system [pink bars in Fig. 4(c)] are smaller than those in the zero-water system

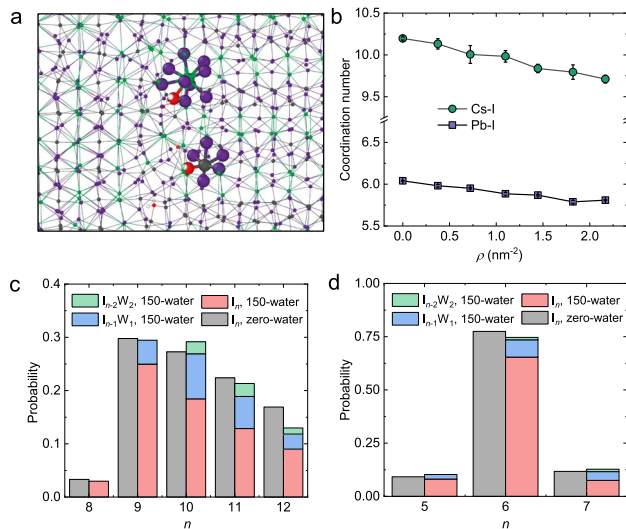


FIG. 4. Water-ion structure at the B/Y interface. (a) MD snapshot of a water molecule binding with Cs (green sphere) and Pb (gray sphere) ions at the B/Y interfaces. (b) Coordination numbers of interfacial Cs and Pb ions with I as a function of ρ . (c) and (d) Distribution of coordination numbers of interfacial (c) Pb and (d) Cs ions in the zero- and 150-water systems.

[gray bars in Figs. 4(c) and 4(d)], and the differences are compensated by 1- and 2-water bindings [blue and green bars in Figs. 4(c) and 4(d)]. The statistical analysis of the binding situations is consistent with the observation that water molecules occupy the positions of I and bind to the cations. The release of I in the interface region facilitates the motion of the ions, thus enhancing the ion diffusion. This mechanism also suggests that other small polar molecules (e.g., DMSO) or anions (e.g., OH⁻) may also accelerate the diffusional phase transitions in perovskite materials.⁵⁴⁻⁵⁶

III. DISCUSSION

We now have gained a comprehensive understanding of the $Y \rightarrow B$ and the reverse $B \rightarrow Y$ phase transitions in CsPbI₃ (Fig. 5). The nucleation and propagation processes of the $B \leftrightarrow Y$ phase transition both follow the C-A-C two-step mechanism.^{14,37,38} During the thermally induced $Y \rightarrow B$ phase transition, the yellow phase destabilizes at a high temperature, forming an amorphous nucleus, which then recrystallizes into the black α -CsPbI₃ [Fig. 5(a), upper panels]. The propagation process of this transition [Fig. 5(a), lower panels] is similar to the nucleation process, whereby the yellow phase melts and transforms into the amorphous interface, which then recrystallizes in the black phase, leading to the growth of black-CsPbI₃. Conversely, the reverse $B \rightarrow Y$ transition follows similar mechanisms but necessitates the aid of water molecules to diminish the nucleation barrier and facilitate the diffusion of interfacial ions [Fig. 5(b)]. The C-A-C transition mechanism has been well-established in metallurgy.⁴³ It has also been observed in the nucleation process of protein crystallization,⁵⁷ as well as in solid-solid phase transitions in colloidal crystals⁵⁸ and PbTiO₃.⁵⁹ This mechanism has been theoretically verified from both kinetic and thermodynamic perspectives.^{60,61} However, prior to this work, there has been no

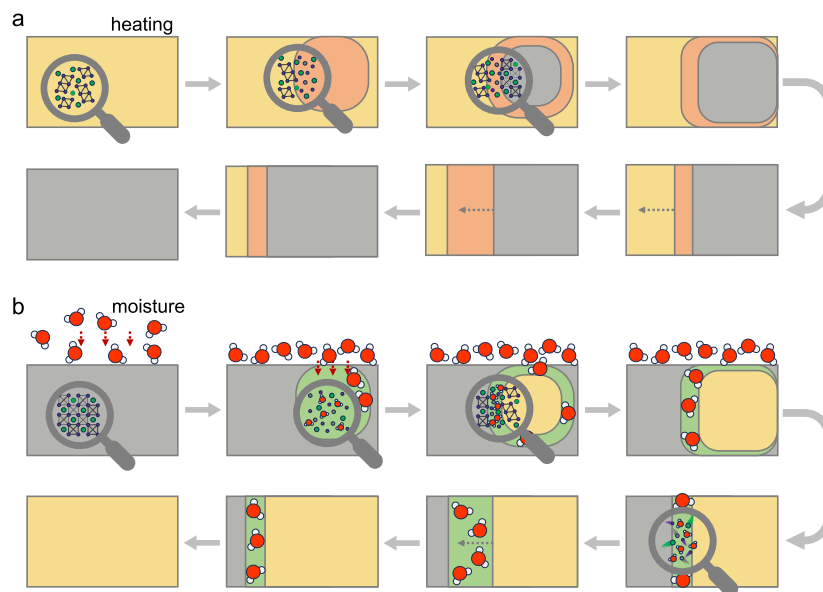


FIG. 5. Microscopic mechanisms of the thermal-induced $Y \rightarrow B$ transition and moisture-induced $B \rightarrow Y$ transition in CsPbI_3 . (a) and (b) Schematic illustrations of the nucleation (upper) and propagation (lower) in (a) $Y \rightarrow B$ and (b) $B \rightarrow Y$ transitions. Yellow, gray, green, and salmon regions indicate the yellow phase, black phase, and amorphous CsPbI_3 with and without water, respectively. Green, gray, purple, red, and white spheres are Cs, Pb, I, O, and H, respectively.

specific validation or comparison of the applicability of the C–A–C and C–C mechanisms in MHP systems.

The mechanism we proposed aligns with the observed characteristics of the $B \leftrightarrow Y$ phase transition in CsPbI_3 and other perovskite systems, showcasing distinct non-martensitic phase transition behaviors.^{14,37,38} Specifically, the transition does not occur simultaneously across all regions within a short timeframe. Instead, it exhibits clearly distinguishable nucleation and propagation processes,⁹ with the latter proceeding along the perpendicular direction of the B/Y interface.²⁰ It is worth noting the close relationship between the C–A–C two-step mechanism and the water-assisted mechanism. First, in the C–A–C mechanism, water interacts with CsPbI_3 by locating at the amorphous nuclei and interfaces. Both DFT calculations and MD simulations have shown that water molecules' intercalation energies in CsPbI_3 crystals are relatively higher than those in amorphous CsPbI_3 (supplementary material and Fig. S11), indicating that water facilitates the phase transitions by entering the amorphous areas. The conclusion that water molecules can easily access the amorphous interface is consistent with the experimental observation that phase transition rates show immediate responses to air humidity.^{9,20} Second, the mechanism by which water molecules accelerate phase transitions by enhancing interfacial ion diffusion aligns with the diffusion-dominant nature of the C–A–C mechanism.^{57,60,61} In a phase transition via the C–A–C pathway, the primary factor influencing the phase transition rate (nucleation barrier) is the ion diffusion at the amorphous regions. As a highly polar solvent, water molecules inevitably increase the diffusion rate of interfacial ions, thereby reducing the phase transition barrier.

Our findings on the microscopic mechanisms of water-assisted $B \rightarrow Y$ phase transitions in CsPbI_3 may also be relevant to other

perovskite materials such as $\text{CsPbBr}_x\text{I}_{3-x}$,¹⁴ CsSnI_3 ,³⁷ and FAPbI_3 .⁴⁸ In the case of the MAPbI_3 system, there is no stable low-temperature non-perovskite structure; however, it degrades into PbI_2 and other by-products under humid conditions.⁶² Cryo-electron microscopy (cryo-EM) experiments have confirmed that this degradation process also follows the C–A–C mechanism, where an amorphous MAPbI_3 hydrate layer initially forms on the surface of MAPbI_3 before decomposing into PbI_2 and gaseous products.⁶³ Additionally, Hidalgo *et al.*⁵⁴ have noted that atmospheric oxygen synergistically accelerates the $B \rightarrow Y$ phase transition in FAPbI_3 , a process that may be accompanied by the formation of $\text{Pb}(\text{IO}_3)_2$. The complex mechanism underlying the cooperative action of O_2 and H_2O in this context requires further in-depth investigation.

The mechanism revealed in this work has the potential to be generalized to different solvents and different solid systems. To achieve solvent/molecule-assisted solid–solid phase transitions, the following conditions should be met: First, the solid–solid phase transition is cumbersome due to a high energy barrier or a complex transition pathway and, therefore, it needs to be accomplished through a two-step C–A–C mechanism. Second, the assisting solvent or molecule should have an appropriate size, making it easier to enter the disordered interface but not to disrupt the crystal structure. Third, the assisting molecules should have a high polarity, ensuring strong interactions with ions in the disordered region, thereby enhancing the diffusion of the interfacial ions.

SUPPLEMENTARY MATERIAL

See the supplementary material for computational methods, force field validation, and more information on the interfacial energy

calculations, force field parameters, additional MD snapshots and trajectories of the CsPbI₃ nanowires and B/Y bulk system, additional data of the phase transition rate and interfacial ion diffusion, and AIMD simulations.

ACKNOWLEDGMENTS

This work was supported by the CAS Pioneer Hundred Talents Program (Grant No. E3291501). J.L. acknowledges the financial support from the Jiangsu Funding Program for Excellent Postdoctoral Talent (Grant No. JB020712). We acknowledge the Suzhou Supercomputing Center (SISCC) for the use of high-performance computing facilities and the associated technical support services.

AUTHOR DECLARATIONS

Conflict of Interest

The authors have no conflicts to disclose.

Author Contributions

Jialin Liu: Data curation (lead); Formal analysis (lead); Investigation (equal); Methodology (equal); Software (lead); Validation (equal); Writing – original draft (equal); Writing – review & editing (equal). **Xiangming Hao:** Formal analysis (supporting); Validation (equal); Writing – review & editing (equal). **Marijn A. van Huis:** Conceptualization (supporting); Investigation (supporting); Writing – review & editing (equal). **Zhaochuan Fan:** Conceptualization (lead); Funding acquisition (lead); Methodology (equal); Supervision (lead); Writing – original draft (equal); Writing – review & editing (equal).

DATA AVAILABILITY

The data that support the findings of this study are available within the article and its [supplementary material](#). The data that support the findings of this study are available from the corresponding author upon reasonable request.

REFERENCES

- 1 J.-W. Lee, S. Tan, S. I. Seok, Y. Yang, and N.-G. Park, “Rethinking the a cation in halide perovskites,” *Science* **375**, eabj1186 (2022).
- 2 S. Tan, T. Huang, I. Yavuz, R. Wang, T. W. Yoon, M. Xu, Q. Xing, K. Park, D.-K. Lee, C.-H. Chen *et al.*, “Stability-limiting heterointerfaces of perovskite photovoltaics,” *Nature* **605**, 268–273 (2022).
- 3 A. Dey, J. Ye, A. De, E. Debroye, S. K. Ha, E. Bladt, A. S. Kshirsagar, Z. Wang, J. Yin, Y. Wang *et al.*, “State of the art and prospects for halide perovskite nanocrystals,” *ACS Nano* **15**, 10775–10981 (2021).
- 4 J. A. Steele, H. Jin, I. Dovgaliuk, R. F. Berger, T. Braeckvelt, H. Yuan, C. Martin, E. Solano, K. Lejaeghere, S. M. Rogge *et al.*, “Thermal un-equilibrium of strained black CsPbI₃ thin films,” *Science* **365**, 679–684 (2019).
- 5 I. Chung, J.-H. Song, J. Im, J. Androulakis, C. D. Malliakas, H. Li, A. J. Freeman, J. T. Kenney, and M. G. Kanatzidis, “CsSnI₃: Semiconductor or metal? High electrical conductivity and strong near-infrared photoluminescence from a single material. High hole mobility and phase-transitions,” *J. Am. Chem. Soc.* **134**, 8579–8587 (2012).

- 6 A. K. Jena, A. Kulkarni, Y. Sanehira, M. Ikegami, and T. Miyasaka, “Stabilization of α -CsPbI₃ in ambient room temperature conditions by incorporating Eu into CsPbI₃,” *Chem. Mater.* **30**, 6668–6674 (2018).
- 7 T. Zhang, M. I. Dar, G. Li, F. Xu, N. Guo, M. Grätzel, and Y. Zhao, “Bication lead iodide 2D perovskite component to stabilize inorganic α -CsPbI₃ perovskite phase for high-efficiency solar cells,” *Sci. Adv.* **3**, e1700841 (2017).
- 8 S. Valastro, G. Mannino, E. Smecca, C. Bongiorno, S. Sanzaro, I. Deretzis, A. La Magna, A. K. Jena, T. Miyasaka, and A. Alberti, “Black-yellow bandgap trade-off during thermal stability tests in low-temperature Eu-doped CsPbI₃,” *Sol. RRL* **6**, 2200008 (2022).
- 9 Z. Lin, Y. Zhang, M. Gao, J. A. Steele, S. Louisia, S. Yu, L. N. Quan, C.-K. Lin, D. T. Limmer, and P. Yang, “Kinetics of moisture-induced phase transformation in inorganic halide perovskite,” *Matter* **4**, 2392–2402 (2021).
- 10 M. Lai, T. Lei, Y. Zhang, J. Jin, J. A. Steele, and P. Yang, “Phase transition dynamics in one-dimensional halide perovskite crystals,” *MRS Bull.* **46**, 310–316 (2021).
- 11 Q. Kong, W. Lee, M. Lai, C. G. Bischak, G. Gao, A. B. Wong, T. Lei, Y. Yu, L.-W. Wang, N. S. Ginsberg, and P. Yang, “Phase-transition-induced p-n junction in single halide perovskite nanowire,” *Proc. Natl. Acad. Sci. U. S. A.* **115**, 8889–8894 (2018).
- 12 G.-W. Chen, B. Wen, J.-S. Xie, L.-K. Chen, and S.-C. Zhu, “Resolving the perovskite degradation mechanism by machine learning potential: The case of CsPbI₃,” *J. Phys. Chem. C* **127**, 11692–11699 (2023).
- 13 G.-Y. Chen, Z.-D. Guo, X.-G. Gong, and W.-J. Yin, “Kinetic pathway of γ -to- δ phase transition in CsPbI₃,” *Chem* **8**, 3120–3129 (2022).
- 14 C. G. Bischak, M. Lai, Z. Fan, D. Lu, P. David, D. Dong, H. Chen, A. S. Etman, T. Lei, J. Sun *et al.*, “Liquid-like interfaces mediate structural phase transitions in lead halide perovskites,” *Matter* **3**, 534–545 (2020).
- 15 Z. Yao, W. Zhao, and S. F. Liu, “Stability of the CsPbI₃ perovskite: From fundamentals to improvements,” *J. Mater. Chem. A* **9**, 11124–11144 (2021).
- 16 Z. Lin, M. C. Folgueras, H. K. Le, M. Gao, and P. Yang, “Laser-accelerated phase transformation in cesium lead iodide perovskite,” *Matter* **5**, 1455–1465 (2022).
- 17 X. Ling, S. Zhou, J. Yuan, J. Shi, Y. Qian, B. W. Larson, Q. Zhao, C. Qin, F. Li, G. Shi *et al.*, “14.1% CsPbI₃ perovskite quantum dot solar cells via cesium cation passivation,” *Adv. Energy Mater.* **9**, 1900721 (2019).
- 18 A. Swarnkar, A. R. Marshall, E. M. Sanehira, B. D. Chernomordik, D. T. Moore, J. A. Christians, T. Chakrabarti, and J. M. Luther, “Quantum dot-induced phase stabilization of α -CsPbI₃ perovskite for high-efficiency photovoltaics,” *Science* **354**, 92–95 (2016).
- 19 F. P. García de Arquer, D. V. Talapin, V. I. Klimov, Y. Arakawa, M. Bayer, and E. H. Sargent, “Semiconductor quantum dots: Technological progress and future challenges,” *Science* **373**, eaaz8541 (2021).
- 20 C.-K. Lin, Y. Zhang, M. Gao, J.-A. Lin, H. K. Le, Z. Lin, and P. Yang, “Controlling the phase transition in CsPbI₃ nanowires,” *Nano Lett.* **22**, 2437–2443 (2022).
- 21 S. Dastidar, C. J. Hawley, A. D. Dillon, A. D. Gutierrez-Perez, J. E. Spanier, and A. T. Fafarman, “Quantitative phase-change thermodynamics and metastability of perovskite-phase cesium lead iodide,” *J. Phys. Chem. Lett.* **8**, 1278–1282 (2017).
- 22 D. B. Straus, S. Guo, and R. J. Cava, “Kinetically stable single crystals of perovskite-phase CsPbI₃,” *J. Am. Chem. Soc.* **141**, 11435–11439 (2019).
- 23 Q. Wang, B. Chen, Y. Liu, Y. Deng, Y. Bai, Q. Dong, and J. Huang, “Scaling behavior of moisture-induced grain degradation in polycrystalline hybrid perovskite thin films,” *Energy Environ. Sci.* **10**, 516–522 (2017).
- 24 S. Cheng and H. Zhong, “What happens when halide perovskites meet with water?,” *J. Phys. Chem. Lett.* **13**, 2281–2290 (2022).
- 25 N. N. Intan and J. Pfaendtner, “Role of surface features on the initial dissolution of CH₃NH₃PbI₃ perovskite in liquid water: An ab initio molecular dynamics study,” *ACS Nano* **17**, 22371–22387 (2023).
- 26 C. Caddeo, M. I. Saba, S. Meloni, A. Filippetti, and A. Mattoni, “Collective molecular mechanisms in the CH₃NH₃PbI₃ dissolution by liquid water,” *ACS Nano* **11**, 9183–9190 (2017).
- 27 L. Zhang, M.-G. Ju, and W. Liang, “The effect of moisture on the structures and properties of lead halide perovskites: A first-principles theoretical investigation,” *Phys. Chem. Chem. Phys.* **18**, 23174–23183 (2016).

- ²⁸E. Mosconi, J. M. Azpiroz, and F. De Angelis, “*Ab initio* molecular dynamics simulations of methylammonium lead iodide perovskite degradation by water,” *Chem. Mater.* **27**, 4885–4892 (2015).
- ²⁹J. Lin, M. Lai, L. Dou, C. S. Kley, H. Chen, F. Peng, J. Sun, D. Lu, S. A. Hawks, C. Xie *et al.*, “Thermochromic halide perovskite solar cells,” *Nat. Mater.* **17**, 261–267 (2018).
- ³⁰F. Tian, W. Feng, B. Xing, X. He, W. A. Saidi, and L. Zhang, “Grain boundaries in methylammonium lead halide perovskites facilitate water diffusion,” *Adv. Energy Sustainability Res.* **2**, 2100087 (2021).
- ³¹W. Kaiser, D. Ricciarelli, E. Mosconi, A. A. Althman, F. Ambrosio, and F. De Angelis, “Stability of tin- versus lead-halide perovskites: *Ab initio* molecular dynamics simulations of perovskite/water interfaces,” *J. Phys. Chem. Lett.* **13**, 2321–2329 (2022).
- ³²D. L. Busipalli, K.-Y. Lin, S. Nachimuthu, and J.-C. Jiang, “Enhanced moisture stability of cesium lead iodide perovskite solar cells—A first-principles molecular dynamics study,” *Phys. Chem. Chem. Phys.* **22**, 5693–5701 (2020).
- ³³K. E. Kweon, J. Varley, T. Ogitsu, L. F. Wan, M. Shelby, Z. Song, R. J. Ellingson, Y. Yan, and J. R. Lee, “Influence of external conditions on the black-to-yellow phase transition of CsPbI₃ based on first-principles calculations: Pressure and moisture,” *Chem. Mater.* **35**, 2321–2329 (2023).
- ³⁴B. Conings, J. Drijkoningen, N. Gauquelin, A. Babayigit, J. D’Haen, L. D’Olieslaeger, A. Ethirajan, J. Verbeeck, J. Manca, E. Mosconi *et al.*, “Intrinsic thermal instability of methylammonium lead trihalide perovskite,” *Adv. Energy Mater.* **5**, 1500477 (2015).
- ³⁵Z. Guo, J. Fu, G. Chen, F. Liu, C. Yu, R. Lu, and W.-J. Yin, “First domino in the structural collapse of perovskite CsPbI₃ and its stabilizing strategies,” *Adv. Funct. Mater.* **34**, 2308246 (2023).
- ³⁶Z. Li, F. Zhou, Q. Wang, L. Ding, and Z. Jin, “Approaches for thermodynamically stabilized CsPbI₃ solar cells,” *Nano Energy* **71**, 104634 (2020).
- ³⁷Y. Wang, J. Liu, J. Wang, and Z. Fan, “Phase stability and transformations in CsSnI₃: Is anharmonicity negligible?,” *J. Phys. Chem. C* **126**, 19470–19479 (2022).
- ³⁸X. Hao, J. Liu, M. Deng, and Z. Fan, “Critical evaluation of five classical force fields for CsPbI₃: Limitations in modeling phase stability and transformations,” *J. Phys. Chem. C* **127**, 20157–20168 (2023).
- ³⁹D. W. Oxtoby, “Nucleation of first-order phase transitions,” *Acc. Chem. Res.* **31**, 91–97 (1998).
- ⁴⁰T. Braeckvelt, R. Goeminne, S. Vandenhoute, S. Borgmans, T. Verstraelen, J. A. Steele, M. B. Roeflaers, J. Hofkens, S. M. Rogge, and V. Van Speybroeck, “Accurately determining the phase transition temperature of CsPbI₃ via random-phase approximation calculations and phase-transferable machine learning potentials,” *Chem. Mater.* **34**, 8561–8576 (2022).
- ⁴¹E. Fransson, J. Wiktor, and P. Erhart, “Phase transitions in inorganic halide perovskites from machine-learned potentials,” *J. Phys. Chem. C* **127**, 13773–13781 (2023).
- ⁴²X. Chen, G. Chen, and W.-J. Yin, “Interphase boundaries and their impact on carrier dynamics in lead halide perovskites,” *J. Phys. Chem. Lett.* **14**, 6459–6463 (2023).
- ⁴³D. A. Porter and K. E. Easterling, *Phase Transformations in Metals and Alloys (Revised Reprint)* (CRC Press, 2009).
- ⁴⁴A. Waleed, M. M. Tavakoli, L. Gu, S. Hussain, D. Zhang, S. Poddar, Z. Wang, R. Zhang, and Z. Fan, “All inorganic cesium lead iodide perovskite nanowires with stabilized cubic phase at room temperature and nanowire array-based photodetectors,” *Nano Lett.* **17**, 4951–4957 (2017).
- ⁴⁵B. Akbali, G. Topçu, T. Guner, M. Ozcan, M. M. Demir, and H. Sahin, “CsPbBr₃ perovskites: Theoretical and experimental investigation on water-assisted transition from nanowire formation to degradation,” *Phys. Rev. Mater.* **2**, 034601 (2018).
- ⁴⁶X. Luo, W. Liu, Z. Wang, T. Lei, P. Yang, and Y. Yu, “Thermally driven phase transition of halide perovskites revealed by big data-powered in situ electron microscopy,” *J. Chem. Phys.* **158**, 134705 (2023).
- ⁴⁷H. Lyu, H. Su, and Z. Lin, “Two-stage dynamic transformation from δ -to α -CsPbI₃,” *J. Phys. Chem. Lett.* **15**, 2228–2232 (2024).
- ⁴⁸P. Ahlawat, A. Hinderhofer, E. A. Alharbi, H. Lu, A. Ummadisingu, H. Niu, M. Invernizzi, S. M. Zakeeruddin, M. I. Dar, F. Schreiber *et al.*, “A combined molecular dynamics and experimental study of two-step process enabling low-temperature formation of phase-pure α -FAPbI₃,” *Sci. Adv.* **7**, eabe3326 (2021).
- ⁴⁹J. R. Espinosa, C. Vega, C. Valeriani, and E. Sanz, “The crystal-fluid interfacial free energy and nucleation rate of NaCl from different simulation methods,” *J. Chem. Phys.* **142**, 194709 (2015).
- ⁵⁰J. R. Espinosa, C. Vega, C. Valeriani, and E. Sanz, “Seeding approach to crystal nucleation,” *J. Chem. Phys.* **144**, 034501 (2016).
- ⁵¹J. Crape, N. Pappireddi, M. Gupta, S. Y. Shvartsman, E. Wieschaus, and M. Wühr, “Evaluating the Arrhenius equation for developmental processes,” *Mol. Syst. Biol.* **17**, e9895 (2021).
- ⁵²C. Eames, J. M. Frost, P. R. Barnes, B. C. O’regan, A. Walsh, and M. S. Islam, “Ionic transport in hybrid lead iodide perovskite solar cells,” *Nat. Commun.* **6**, 7497 (2015).
- ⁵³U.-G. Jong, C.-J. Yu, G.-C. Ri, A. P. McMahon, N. M. Harrison, P. R. Barnes, and A. Walsh, “Influence of water intercalation and hydration on chemical decomposition and ion transport in methylammonium lead halide perovskites,” *J. Mater. Chem. A* **6**, 1067–1074 (2018).
- ⁵⁴Y. Jo, K. S. Oh, M. Kim, K.-H. Kim, H. Lee, C.-W. Lee, and D. S. Kim, “High performance of planar perovskite solar cells produced from PbI₂(DMSO) and PbI₂(NMP) complexes by intramolecular exchange,” *Adv. Mater. Interfaces* **3**, 1500768 (2016).
- ⁵⁵D. Ricciarelli, W. Kaiser, E. Mosconi, J. Wiktor, M. W. Ashraf, L. Malavasi, F. Ambrosio, and F. De Angelis, “Reaction mechanism of photocatalytic hydrogen production at water/tin halide perovskite interfaces,” *ACS Energy Lett.* **7**, 1308–1315 (2022).
- ⁵⁶Q. Lin, S. Bernardi, B. Shabbir, Q. Ou, M. Wang, W. Yin, S. Liu, A. S. Chesman, S. O. Füller, G. Si, N. Medhekar, J. Jasieniak, A. Widmer-Cooper, W. Mao, and U. Bach, “Phase-control of single-crystalline inorganic halide perovskites via molecular coordination engineering,” *Adv. Funct. Mater.* **32**, 2109442 (2022).
- ⁵⁷P. R. t. Wolde and D. Frenkel, “Enhancement of protein crystal nucleation by critical density fluctuations,” *Science* **277**, 1975–1978 (1997).
- ⁵⁸Y. Peng, F. Wang, Z. Wang, A. M. Alsayed, Z. Zhang, A. G. Yodh, and Y. Han, “Two-step nucleation mechanism in solid–solid phase transitions,” *Nat. Mater.* **14**, 101–108 (2015).
- ⁵⁹V. I. Levitas, Z. Ren, Y. Zeng, Z. Zhang, and G. Han, “Crystal–crystal phase transformation via surface-induced virtual premelting,” *Phys. Rev. B* **85**, 220104 (2012).
- ⁶⁰V. I. Levitas, “Crystal–amorphous and crystal–crystal phase transformations via virtual melting,” *Phys. Rev. Lett.* **95**, 075701 (2005).
- ⁶¹V. I. Levitas, B. F. Henson, L. B. Smilowitz, and B. W. Asay, “Solid–solid phase transformation via virtual melting significantly below the melting temperature,” *Phys. Rev. Lett.* **92**, 235702 (2004).
- ⁶²J. Yang, B. D. Siempelkamp, D. Liu, and T. L. Kelly, “Investigation of CH₃NH₃PbI₃ degradation rates and mechanisms in controlled humidity environments using in situ techniques,” *ACS Nano* **9**, 1955–1963 (2015).
- ⁶³Y. Li, W. Zhou, Y. Li, W. Huang, Z. Zhang, G. Chen, H. Wang, G.-H. Wu, N. Rolston, R. Vila *et al.*, “Unravelling degradation mechanisms and atomic structure of organic–inorganic halide perovskites by Cryo-EM,” *Joule* **3**, 2854–2866 (2019).
- ⁶⁴J. Hidalgo, W. Kaiser, Y. An, R. Li, Z. Oh, A.-F. Castro-Méndez, D. K. LaFollette, S. Kim, B. Lai, J. Breternitz *et al.*, “Synergistic role of water and oxygen leads to degradation in formamidinium-based halide perovskites,” *J. Am. Chem. Soc.* **145**, 24549–24557 (2023).